Integration of in situ experiments and numerical simulations to reveal the physicochemical circumstances of organic and inorganic precipitation at a thermal spring

Petra Kovács-Bodor[a*], Dóra Anda[b], Laura Jurecska[b], Mihály Óvári[c], Ákos Horváth[d], Judit Makk[b], Vincent Post[e], Imre Müller[a], Judit Mádl-Szőnyi[a]

[a] József and Erzsébet Tóth Endowed Hydrogeology Chair, Department of Physical and Applied Geology, ELTE Eötvös Loránd University, Pázmány Péter stny. 1/C., H-1117, Budapest, Hungary

[b] Department of Microbiology, ELTE Eötvös Loránd University, Pázmány Péter stny. 1/C., H-1117, Budapest, Hungary

[c] MTA Centre for Ecological Research, Danube Research Institute, Karolina út 29., H-1113, Budapest, Hungary

[d] Department of Nuclear Physics, ELTE Eötvös Loránd University, Pázmány Péter stny. 1/A., H-1117, Budapest, Hungary

[e] Federal Institute for Geosciences and Natural Resources, Hannover, Germany

* corresponding author: Petra Kovács-Bodor, petra.bodor28@gmail.com, ELTE Eötvös Loránd University, Pázmány Péter stny. 1/C., H-1117, Budapest, Hungary

email addresses: petra.bodor28@gmail.com (P. Kovács-Bodor), andadora@caesar.elte.hu (D. Anda), jurecskalaura@gmail.com (L. Jurecska), ovari.mihaly@okologia.mta.hu (M. Óvári), akos@ludens.elte.hu (Á. Horváth), makkjudit@gmail.com (J. Makk), Vincent.Post@bgr.de (V. Post), imremuller40@gmail.com (I. Müller), szjudit@ludens.elte.hu (J. Mádl-Szőnyi)

Abstract

Organic and inorganic precipitates are both characteristic in the active hypogenic karst area of Buda Thermal Karst in Hungary. As an active system, it is a good natural laboratory to study ongoing precipitation processes. Because of anthropogenic influence and the complexity of spring environments, it is challenging to reveal all the governing factors in the process of precipitation. In situ experiments, i.e. artificially controlled natural systems simplify the complexity by adding, excluding or stabilizing influencing parameters during the experiment.

CO_2 degassing drives changes in the physicochemical parameters of spring waters from the discharge along their flow path. The rate and spatial extension of these changes depend on local hydrogeological, geological, climatic, topographical etc. factors, affecting precipitation processes.

In this study, two one-day-long in situ experiments were executed to examine the physicochemical parameter changes of thermal water in a tunnel. The integration of the results with reactive transport models revealed the physicochemical processes of ingassing and degassing and predicted CaCO3 precipitation along the flow path. Small-scale roughness of the channel surface seemed to further influence pH and concentration of HCO3-. After six weeks of thermal water flowing, organic precipitate (biofilm) formed close to the discharge and then, with a sharp change, inorganic precipitate (calcite) dominates a bit further from the discharge.

In situ experiments and connected numerical simulations revealed the role of CO_2 degassing and calcite precipitation in the changes of physicochemical parameters, but organic precipitates also have to be considered near the discharge.

Keywords

thermal water; in situ experiment; physicochemical parameters; reactive transport modelling; organic precipitation; inorganic precipitation

Acknowledgement

This work was supported by the National Research Development and Innovation Office (NKFIH 101356). The authors would like to thank the permission and the help of Budapest Spa Plc. and the management of Gellért Spa. The measurements would not have been possible without the assistance of the Geology BSc, MSc and PhD students of Eötvös Loránd University. The scientific discussions with Andrea Mindszenty are highly appreciated. Both in the field and in the laboratory, László Szikszay has provided essential help. Thanks are also due to the Departments of Nuclear Physics, Microbiology, Physical Geography, Meteorology, Analytical Chemistry and the Imre Müller and Heinz Surbeck Hydrogeology Laboratory of Eötvös Loránd University for the various measurements which were required. Special thanks to Heinz Surbeck for providing the alpha spectrometer to measure the radionuclides. Thanks also to András Hegedűs and Katalin Csondor for their professional work on the photos.

1. Introduction

Changes in the physicochemical parameters of springs are observed from their points of outflow along their flow paths. The main driving force of these changes is the degassing of CO_2 due to the significant difference between the partial pressure of CO_2 in the air and in the water. One consequence of CO_2 escape is an increase in pH. Additionally, the oxidative environment, i.e. the air causes a rise in the dissolved oxygen content of the water. The rate and spatial extension of the variations depends on many factors, such as the change in pressure, the initial physicochemical parameters, the flow velocity and depth of the water, parameters related to the air, and the irregularities of the bottom of the spring or stream bed,

i.e. turbulence (Chen et al., 2004; Dandurand et al., 1982; Hammer et al., 2008; Herman & Lorah, 1986, 1987; Hoffer-French & Herman, 1989, 1990; Lorah & Herman 1988, 1990; Nordstrom et al., 2005; Zhang et al., 2001).

The aquatic chemistry of the outflowing water is dependent on the groundwater flow system feeding the spring (Tóth, 1963). In the case of the discharge of a regional groundwater flow system, thermal water rises to the surface, and this is characterized by a low dissolved oxygen content, neutral or acidic pH, a high Total Dissolved Solid (TDS) content, elevated temperature and, usually, a high concentration of CO_2 (Goldscheider et al., 2010; Mádl-Szőnyi and Tóth, 2015; Tóth, 1963). As a consequence of these characteristics, the gradient between the discharging thermal water and the air is high, so the physicochemical parameters change abruptly closer to the outflow than in the case of lukewarm and cold springs. The 38.5–93 °C thermal waters in Yellowstone National Park display remarkable variations in the parameters over the first 6–30 meters from the outflow (Nordstrom et al., 2005). In the case of colder waters (9.3–35 °C), however, at locations with similar surface temperatures, a greater distance from the outflow (ranging from 47 m up to as far as 10 km) is required for such differences to be observed (Amundson and Kelly, 1988; Dandurand et al., 1982; Das and Mohanti, 2015; Dreybrodt el al., 1992; Herman & Lorah, 1986, 1987; Hoffer-French and Herman, 1989, 1990; Lorah and Herman 1988, 1990).

The latitudinal and altitudinal location of a given spring discharge is another crucial factor in defining the gradient between the water and the air. The temperature, humidity, air pressure, seasonality, daily variations of these parameters are further factors influencing changes in the physicochemical parameters of the flowing water, so as the density and type of vegetation (e.g. Das & Mohanti, 2015; Herman & Lorah, 1986; Hoffer-French & Herman, 1989, 1990).

90 It is a special case when the spring discharges into a cave. There are no or quite smoothened
91 seasonality and daily variations in air conditions in caves compared to the outside air.
92 Furthermore, in the absence of light, there is no photosynthetic vegetation, but there are plenty
93 of nutrients for chemoautotrophic and chemolithoautotrophic bacteria, which inhabit the walls
94 and the water, usually forming biofilms (e.g. Engel et al. 2001; Sarbu et al., 1996). Biofilms
95 also form in subaerial springs (e.g. Amundson & Kelly, 1998; Das & Mohanti, 2015;
96 Nordstrom et al. 2005). The bacteria influence their environment via metabolization and
97 therefore, take part in the processes of dissolution and precipitation (e.g. Ehrlich, 2001).

98 Carbonates are also common phenomena in caves and springs. The increasing pH of water
99 causes a rise in the saturation index with respect to calcite ($SI_{calcite}$) and after reaching the
100 appropriate state of supersaturation, $CaCO_3$ precipitates. Biofilms and carbonates often occur
101 together, connected to the same water body, and characterized by the same water chemistry.
102 Because of that, and the complexity of natural spring systems, it is challenging to measure and
103 take into consideration all the governing factors in the process of precipitation. Laboratory
104 experiments are often executed to study the evolution of precipitates and the effects of
105 specific parameters. However, it is not possible to make such a complex system in the
106 laboratory, what exists in the nature. In situ experiments, i.e. artificially controlled natural
107 systems provide a key solution in overcoming these problems. Parameters can be added,
108 excluded or stabilized during the in situ experiment. The changes of the water chemistry and
109 the formation of the precipitates can be followed in time and space.

110 Based on these preliminary considerations, an in situ experiment was conducted in the active
111 hypogenic karst area of Buda Thermal Karst (BTK) in Hungary, where biofilm formation and
112 carbonate precipitation are active processes (Erőss, 2010; Mádl-Szőnyi and Erőss, 2013). The
113 direct observation of ongoing precipitation processes is possible near the surface in thermal

114 spring caves and hypogenic caves (Erőss, 2010), and thus providing an excellent natural
115 laboratory. The thermal springs of the BTK are anthropogenically controlled, so in situ
116 experiments cannot be made at these locations. But there is a canal in the artificial tunnel of
117 Gellért Hill, which is located close to the thermal water discharge in the south part of the
118 BTK. Here thermal water can be directed into a trapezoid canal, simulating thermal spring
119 discharge in a cave environment. The known and constant initial volume discharge, the easily
120 measurable water chemistry along the flow path and the regular canal profile provide good
121 input data to a reactive transport model. The integration of in situ experiment and numerical
122 simulation gives a detailed picture of the changing physicochemical parameters and the
123 underlying biogeochemical processes.

124 The aim of the study was to examine the rate and spatial extension of the physicochemical
125 parameter changes of flowing thermal water via an in situ experiment in the "artificial cave"
126 of a natural laboratory to reveal the circumstances of the evolution of organic and inorganic
127 precipitation in advance of their formation. Furthermore, to examine the distribution of
128 radionuclides and trace elements along the flow path of the thermal water, before the
129 adsorbing precipitates form. Beside the measurements, reactive transport modelling was used
130 to simulate the main chemical reactions along the flow path of the thermal water.

131 ## 2. The study area

132 ### 2.1 Gellért Hill

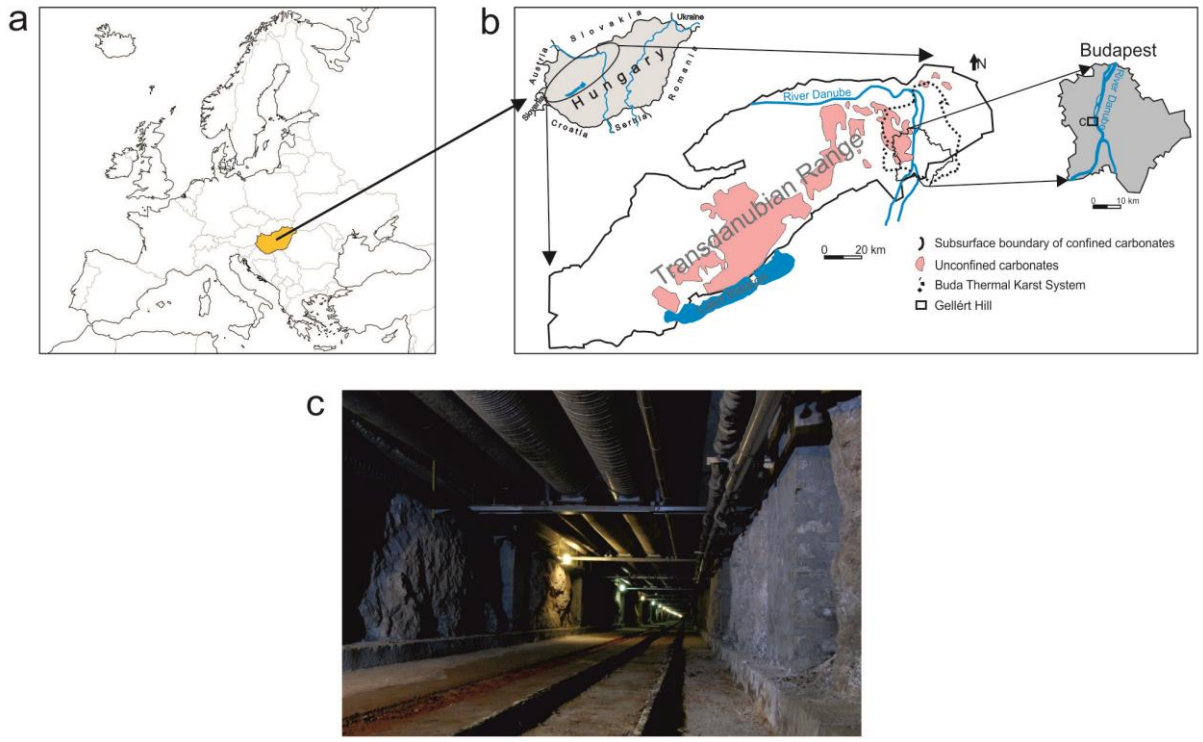

133

134 **Fig. 1** (**a**) Location of Hungary in Europe, (**b**) the study area in the Transdanubian Range
135 (modified after Fülöp in Haas, 2001 and Mádl-Szőnyi et al., 2001) and (**c**) the Gellért tunnel

136 The BTK is the regional discharge area of a thick carbonate system lying on the boundary of
137 confined and unconfined carbonates (Mádl-Szőnyi and Tóth, 2015). The BTK is situated on
138 the northeastern edge of this carbonate system, the Transdanubian Range (Fig. 1a, b).
139 Hydraulic and hydrochemical studies and the radionuclide analysis of the BTK have assisted
140 in the delineation of the flow components of the discharge area (Erhardt et al., 2017; Erőss et
141 al., 2012; Mádl-Szőnyi et al., 2017a, b). In the Gellért Hill area, only thermal springs,
142 originating from regional groundwater flow systems discharge. These waters are characterized
143 by not only fresh karst water, but by some additional basinal fluid component from the
144 confined part. The discharging thermal water has elevated concentrations of HCO_3^-, Ca^{2+},
145 Mg^{2+} and SO_4^{2-} (Erőss, 2010; Kovács and Erőss, 2017). The basinal fluids, on the other hand,
146 are responsible for the Na^+, Cl^-, Ra^{2+}, CO_2, H_2S, H_2SiO_3 and trace element content of the
147 discharging water (Mádl-Szőnyi and Tóth, 2015; Mádl-Szőnyi et al., 2017a) (Fig. 2).

148 Associated with the discharge of groundwater flow systems, springs, thermal caves (e.g. Leél-
149 Őssy, 1995; Leél-Őssy and Surányi, 2003; Takács-Bolner and Kraus, 1989), inorganic and
150 organic precipitates are to be found in this specific hydrogeologic environment (Erőss, 2010;
151 Mádl-Szőnyi and Erőss, 2013). It has been discovered that biofilms are formed where the
152 discharging reduced thermal water become oxidized, i.e. meets the air (Borsodi et al., 2012;
153 Erőss et al. 2012). Bacteria, inhabiting the biofilms, take part mainly in the iron and sulphur
154 cycle via iron (FeII)/sulphur-oxidation or iron(FeIII)/sulphate-reduction (Anda et al. 2014;
155 Borsodi et al., 2012; Makk et al. 2016). Furthermore, biofilms in spring caves and springs can
156 adsorb ^{226}Ra from the water and are responsible for the elevated ^{222}Rn content of thermal
157 springs in the BTK, (Erőss et al., 2012), similar phenomena have been observed in Japan
158 (Fujisawa and Tazaki, 2003; Nagai et al., 2001; Tazaki, 2009) and in Switzerland (Gainon et
159 al., 2007). Trace elements also tend to accumulate in biofilms (Dobosy et al., 2016; Le Guern
160 et al., 2003).

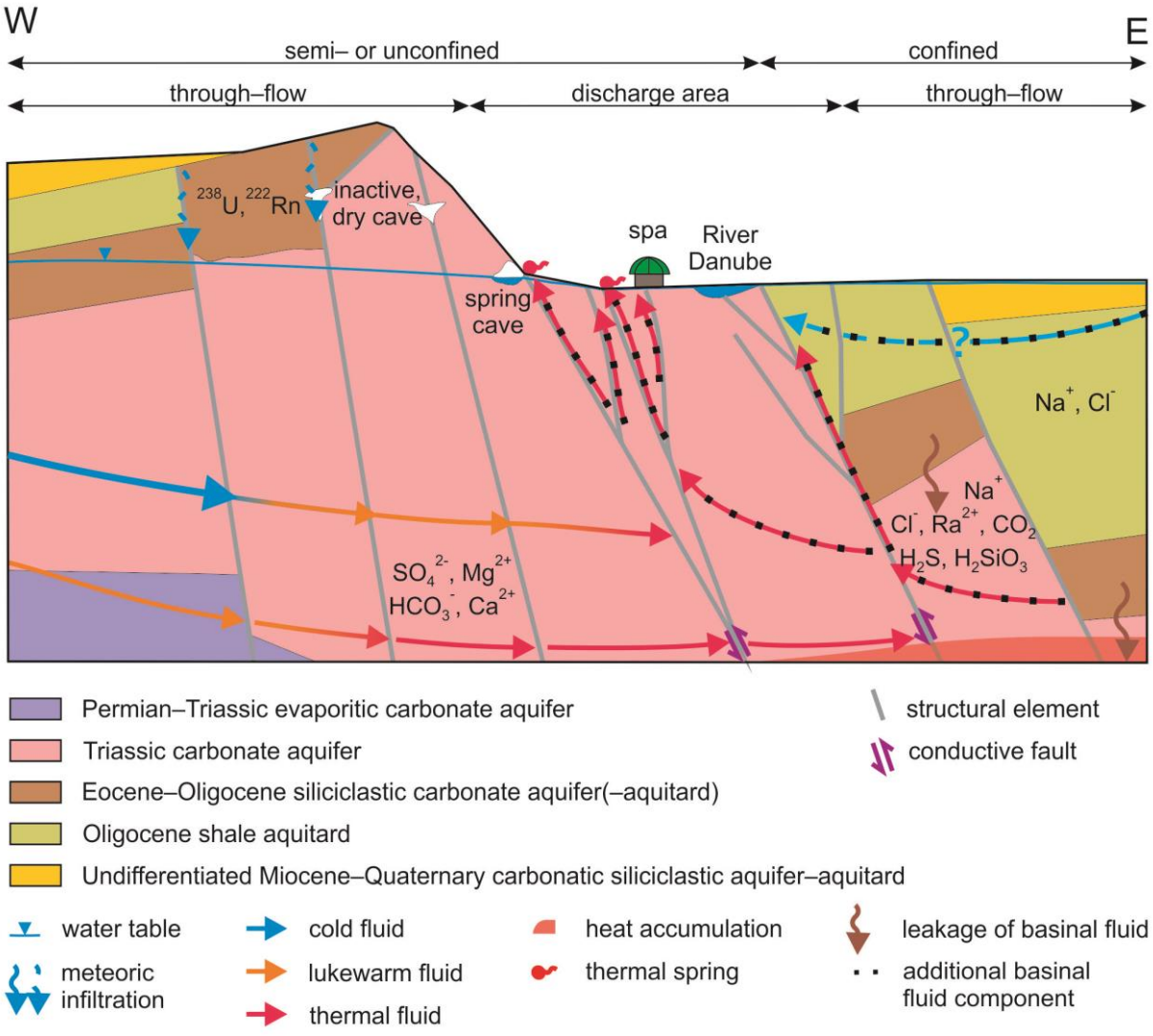

Fig. 2 Conceptual hydrogeological model of the Gellért Hill discharge area (Erőss, 2010 modified by Mádl-Szőnyi et al., 2017a)

2.2 Location of the in situ experiment

A canal in an artificial tunnel in Gellért Hill was the location of the in situ experiment. The tunnel was built between 1969 and 1978 to act as a gallery and to supply the spas of Buda along the River Danube with unpolluted thermal water. The tunnel is 1100 metres long and situated by 2–3 meters above the groundwater level. It connects three spas (Fig. 3a).

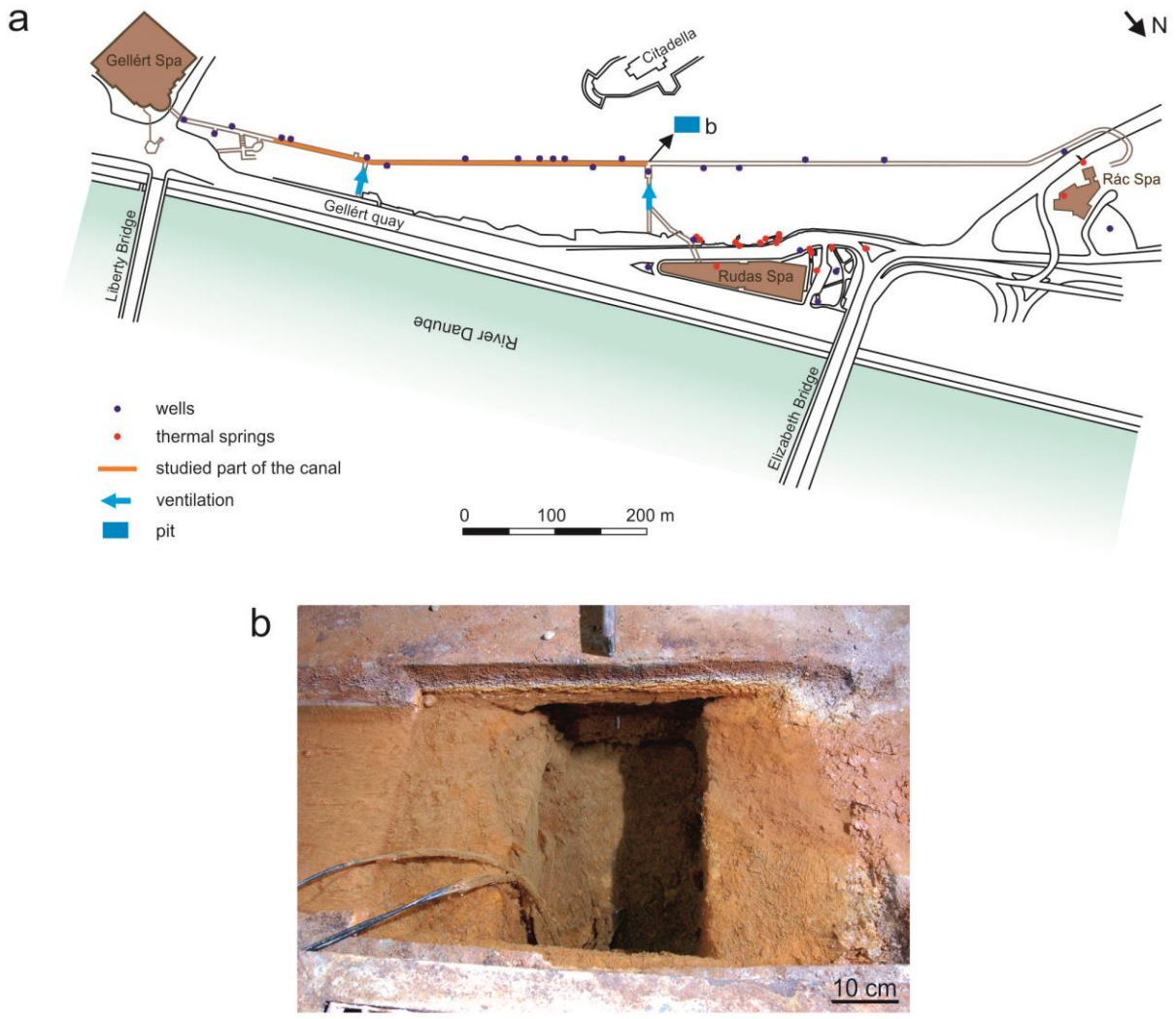

Fig. 3 (**a**) Route of the Gellért tunnel, with the location of spas, wells, thermal springs, ventilation ducts and the pit and (**b**) the pit

The groundwater and Danube are hydraulically connected, so when the river floods, the river water pushes the discharge of thermal water down into river bed, causing the shifting of this extra thermal water discharge to the river bank (Alföldi et al., 1968; Schafarzik, 1920; Somogyi, 2009; Striczki, 2010 etc.). Consequently, during floods the tunnel is submerged under thermal water. To facilitate access to the tunnel during these high-water episodes and control the outflowing water, pits (Fig. 3b) and a trapezoid canal (average size: bases - 27 and 39 cm, legs - 9 and 7 cm) have been excavated into the concrete floor of the tunnel.

A 400m long section of the canal was studied in the course of the in situ experiment, because thermal water discharges in the area of Gellért Hill at a temperature of 31.4–46.7 °C (Erőss et al. 2012), so the gradient is high and fast changes are to be expected in the physiochemical parameters of the water, surely stabilizing in the 400m long section.

Based on measurements made within the in situ experiment, two main factors influence the air temperature in the tunnel (Weidinger et al., 2016). The first is the presence of the district heating pipes of the city, which are attached to and follow the ceiling of the tunnel. The second is the location of various junctions and ventilation ducts. In the studied 400m long section of the tunnel, there are two places where fresh air can enter. One is where the thermal water outflows from the pit (at the Rudas Spa junction) and the other is at a distance of around 300m from the pit (Fig. 3).

3. Data and methods

3.1 Experimental settings

The in situ experiments were carried out when the water level of the Danube was relatively low, so the effects of flood could be excluded. To provide thermal water outflow, a pump (Barwig BWV 01 low voltage submersible pump) was inserted into the pit (width*length*depth: 25*35*39 cm) (Fig. 3b) at the Rudas Spa junction. This pump ensured a constant and manageable level of water discharge.

The one-day-long experiment was performed on two separate occasions, 23rd March 2016 and 22nd April 2016. On both occasions, pumping was started a few hours before the measurements to ensure the water filled the entire examined length (400 m) of the canal. Later on, the experiment was repeated for 6 weeks to study the thermal water precipitates, to validate the results of the integration of one-day-long experiments and numerical simulations.

3.2 Measured and sampled parameters, sampling strategy and procedure

On both experimental occasions, parameters were measured at defined distances from the pit, i.e. from the outflow of the thermal water. Those parameters were measured which can influence precipitation processes or can be affected by the precipitates (temperature, pH, specific electric conductivity, dissolved oxygen content, concentration of anions, cations and trace elements, activity of ^{226}Ra and ^{222}Rn). The location of the March sampling points may be seen in Figure 4a. The sampling density was more frequent over the first 50 m based on the literature, i.e. the physicochemical parameters of the thermal water change fast close to the outflow. Temperature, specific electric conductivity, pH, dissolved oxygen content, concentration of HCO_3^- and water discharge were recorded on site. Furthermore, samples were collected for laboratory measurement of major ion analysis (Ca^{2+}, Mg^{2+}, Na^+, K^+, Cl^-, CO_3^{2-}, SO_4^{2-}) from the pit and at distances of 50 and 400 metres in order to obtain a general overview of the changes in ion concentrations. As calcite is the main evolving precipitate in the area, only Ca^{2+} and HCO_3^- were measured on site at every sampling point.

In the course of the second experimental session, the location of sampling points (Fig. 4b) was modified based on the results of the first one. The number of measured parameters was also increased. Besides the parameters measured earlier, samples were also collected for the laboratory measurement of ^{226}Ra and ^{222}Rn from all sampling points and for the analysis of trace elements from the pit. As water temperature is the parameter most sensitive to the variations of air conditions, air temperature was also monitored during the second sampling session to understand the effects of the heating pipes and the ventilation ducts.

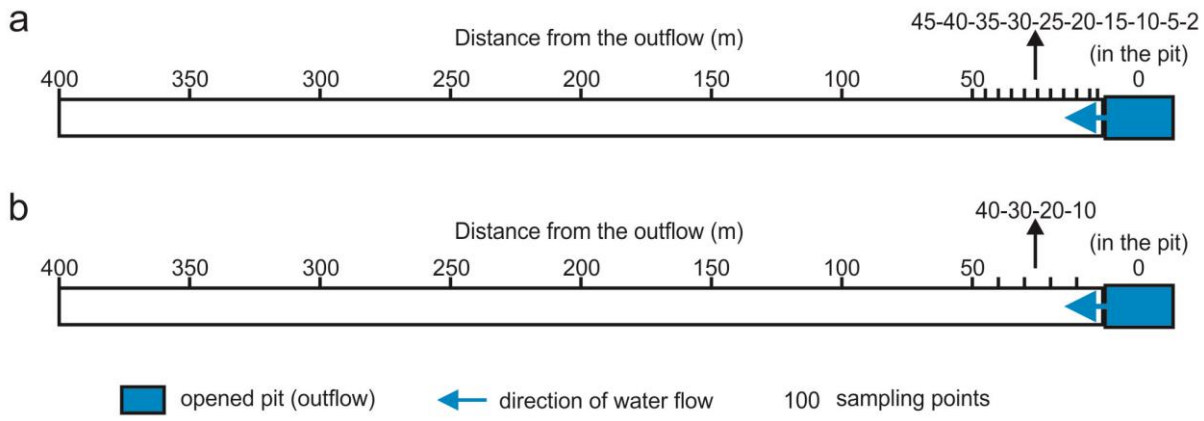

223

224 **Fig. 4** Sampling points of the in situ experiment along the flow path on (**a**) 23rd March and (**b**)

225 22nd April 2016

226 **3.3 Applied methods**

227 The applied methods, the accuracy/detection limit of the measurements and the laboratories

228 are summarized in Table 1. The major ions were determined with the usual analytical

229 laboratory techniques, following standard methods (Eaton et al., 2005). For these

230 measurements, samples were collected in 1.5 l PET bottles with no free head space and were

231 kept cool until the analysis (within 1–2 days).

232 To determine ^{222}Rn activity, 10 ml samples were injected into glass vials containing 10 ml

233 Optifluor-O cocktail at the site. The cap of the vial was additionally wrapped with parafilm.

234 The activity was determined within 24 hours because of the short half-life of the isotope (3.82

235 days).

236 For ^{226}Ra sampling, 0.25 l PET bottles were used. The radionuclides were measured using

237 Nucfilm discs (Surbeck, 2000). The samples were kept cool between the sampling and the

238 measurements (within 3–4 weeks).

239 **Table 1** Summary of the measured parameters, methods, accuracies/detection limits and

240 laboratories

Parameter	Method	Accuracy/detection limit	Laboratory
Temperature, specific electric conductivity, pH, dissolved oxygen	HQ40d Multi-Parameter Meter	±2 % for specific electric conductivity ±0.01 for pH ±0.1 mg/l for dissolved oxygen	On site
Ca^{2+}	EDTA titrimetric method (ASTM 3500-Ca D)	±2 %	On site
HCO_3^-	alkalinity titration (ASTM 2320 B)	±2 %	On site
Na^+, K^+	Flame emission photometry (ASTM 3500-Na D, ASTM 3500-K D)	±2 %	Department of Physical Geography, ELTE*
Mg^{2+}	EDTA titrimetric method (ASTM 3500-Mg E)	±2 %	Department of Microbiology, ELTE*
Cl^-	Argentometric titrimetry (ASTM 4500-Cl^--B)	±2 %	Department of Microbiology, ELTE*
SO_4^{2-}	Turbidimetric method (ASTM 4500-SO_4^{2-}-E)	±5 %	Department of Microbiology, ELTE*
^{222}Rn	Liquid scintillation method TRICARB 1000 TR	min. 3 Bq/l	Department of Atomic Physics, ELTE*
^{226}Ra	Alpha spectrometry (Surbeck, 2000)	min. 10 mBq/l	Imre Müller and Heinz Surbeck Hydrogeology Laboratory of the Department of Physical and Applied Geology, ELTE*
Trace elements	ICP-MS (Element2, ThermoFinnigan, Bremen, Germany)		Department of Analytical Chemistry, ELTE*
Air temperature	Voltcraft DL-120TH	±1 °C	On site

* Eötvös Loránd University

241

242 On the second occasion, samples of trace elements for analysis were collected in 15 ml
243 polypropylene tubes. At each sampling point, both an unfiltered and a 0.2 μm filtered sample
244 were taken, in order to determine the distribution of the trace elements between the dissolved
245 and suspended matter. The samples were acidified with HNO_3 on site to ensure a pH of <1.

After adding 10 µg/l indium internal standard, the analysis was carried out with the use of inductively coupled plasma-mass spectrometry (ICP-MS). Quantification was performed following the external calibration method.

Water discharge was measured by scaling at the outflow of thermal water. Along the flow path of the canal, discharge was calculated from flow velocities determined by surface floating method and trapezoid sections of the canal.

Air temperature was measured about 20 centimetres above the bottom of the tunnel.

To support the interpretation of the concentration patterns measured in March and April, reactive transport modelling was conducted using the PHREEQC code (Parkhurst and Appelo, 2013). The reactions considered were similar to those in the work of Keppel et al. (2012) in their study of spring outflow into a wetland, i.e. gas exchange between the water and atmosphere and calcite precipitation. In the present study, the degassing of CO_2 and ^{222}Rn and the ingassing of O_2 were modelled using the rate expression, Eq. (1):

$$r = k(m - m_{eq}) \quad (1)$$

where r is the rate of gas transfer between the water and the air in the tunnel (M/s, where M is molality), k is the gas exchange rate constant (1/s), m is the concentration of the gas (M), and m_{eq} is the concentration of the gas in equilibrium with the water at the prevailing temperature (M). The latter value is calculated using PHREEQC. Calcite precipitation was modelled using the kinetic rate equation developed by Plummer et al. (1978). This rate expression is implemented in the standard database of PHREEQC (phreeqc.dat) used in this study. The gas exchange rate constant k depends on several factors, including turbulent dissipation at the air-water interface, water depth, flow velocity, the kinematic viscosity of the water, and the diffusion rate of the gas (Raymond et al., 2012). While theoretical relationships are available

to calculate *k*, poor agreement has been reported between these and values of *k* measured in tracer injection experiments (Genereux & Hamond, 1992). In the present study, the value of *k* was therefore optimized by fitting the model to the measured concentrations.

The morphology of the evolved precipitates was examined by scanning electron microscopy (SEM). The samples were filtered onto 0.2 μm polycarbonate filter (Millipore) fixed in glutaraldehyde (5 % in 0.1 M phosphate buffer) for 4–5 hours at room temperature. The fixed samples were rinsed twice with phosphate buffer solution (pH 7), shock frozen in liquid nitrogen and freeze-dried (until 2 x 10^{-2} mbar, at -60 °C for 6–8 h). After lyophilization, the dried samples were mounted on metal stubs, and sputter-coated with gold. The samples were examined using an EVO MA 10 Zeiss scanning electron microscope at an accelerating voltage of 10 kV.

The mineral composition of the crystalline precipitates was investigated by X-ray powder diffractometer (XRD), using a Siemens D5000 type device (Bragg-Brentano setup, Cu radiation).

4. Results of the in situ experiment

4.1 Field parameters and major ions

Water temperature decreased overall from 36 to 32.6 °C in the first session, and from 36.9 to 31.5 °C in the second. In the first occasion, the temperature dropped from 36 °C to 30.8 °C over the 200m, and then increased to 32.6 °C. In the second session, the water temperature dropped (36.9–33.2 °C) over the first 150m, then increased (33.2–34.2 °C) by 250m, and decreased again (34.2–31.5 °C) (Fig. 5).

290 The air temperature ranged from 35 to 37 °C (Fig. 5). 50m from the pit it increased, then it
291 became stable, decreasing after 300 m.

292 The change in pH was very sharp. The thermal water in the pit was slightly acidic (6.84; 6.79)
293 and it changed to alkaline (8.05; 8.42) between the two ends. In the March sampling session,
294 pH increased rapidly, 6.84 to 7.84, between the pit and the 25m point. Between 25 and 50 m,
295 it was stable at around 7.8. Then it increased slightly to 8.22 and finally dropped to 8.05 at the
296 end of the canal. In April, pH increased abruptly from 6.79 to 8.23 between the pit and the
297 80m point. After 80m, it barely changed (Fig. 5).

298 Dissolved oxygen increased along the flow path on both occasions. In the first case, it was 1.7
299 mg/l at the pit and 7.3 mg/l at 400m. It changed rapidly between the pit and 100m, then at a
300 lower rate. On the second occasion, it changed from 0.9 mg/l to 7.5 mg/l, with an abrupt rise
301 between the pit and the 100m point (Fig. 5).

302 Specific electric conductivity decreased from 2059 μS/cm to 1666 μS/cm in March and from
303 2011 μS/cm to 1732 μS/cm in April. In both sampling sessions the greater part of the drop in
304 specific electric conductivity took place over the first 100 m (Fig. 5).

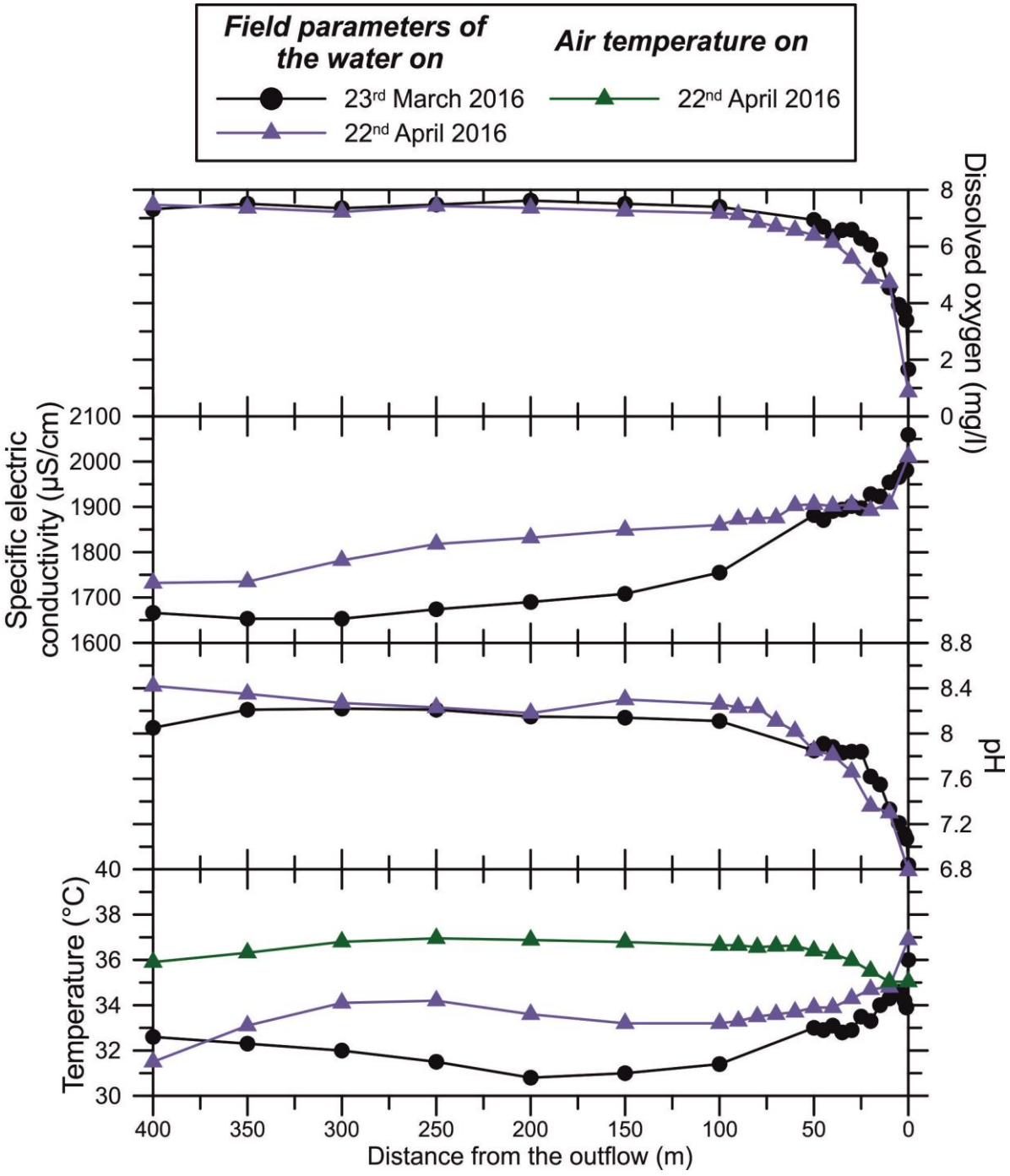

305

306 **Fig. 5** Variations in the field parameters along the flow path for the two occasions (error of

307 measurements: DO: ±0.1 mg/l, EC: ±2 %, pH: ±0.01, T: ±1 °C)

308 At the outflow of the thermal water, the volume discharge was an average of $1.8*10^{-4}$ m^3/s in

309 March and $1.2*10^{-4}$ m^3/s in April. The measured volume discharge was $2.14*10^{-4}$ m^3/s in the

310 canal in March and fell between $3.57*10^{-5}$ and $3.61*10^{-4}$ m^3/s in April.

311 The concentration of HCO_3^- and Ca^{2+} decreased along the whole flow path from 531 to 295
312 mg/l and from 173 to 101 mg/l, respectively in March. In April, the concentration of HCO_3^-
313 and Ca^{2+} decreased from 554 to 331 and from 170 to 98 mg/l, respectively (Fig. 6). The
314 concentrations of the other major ions did not change significantly along the flow path (Cl^-
315 (147–153 mg/l), Mg^{2+} (58–58 mg/l), Na^+ (119–128 mg/l) and K^+ (17–19 mg/l)) according to
316 the widely-spaced measurements (at 0, 50 and 400 m) (Table 2).

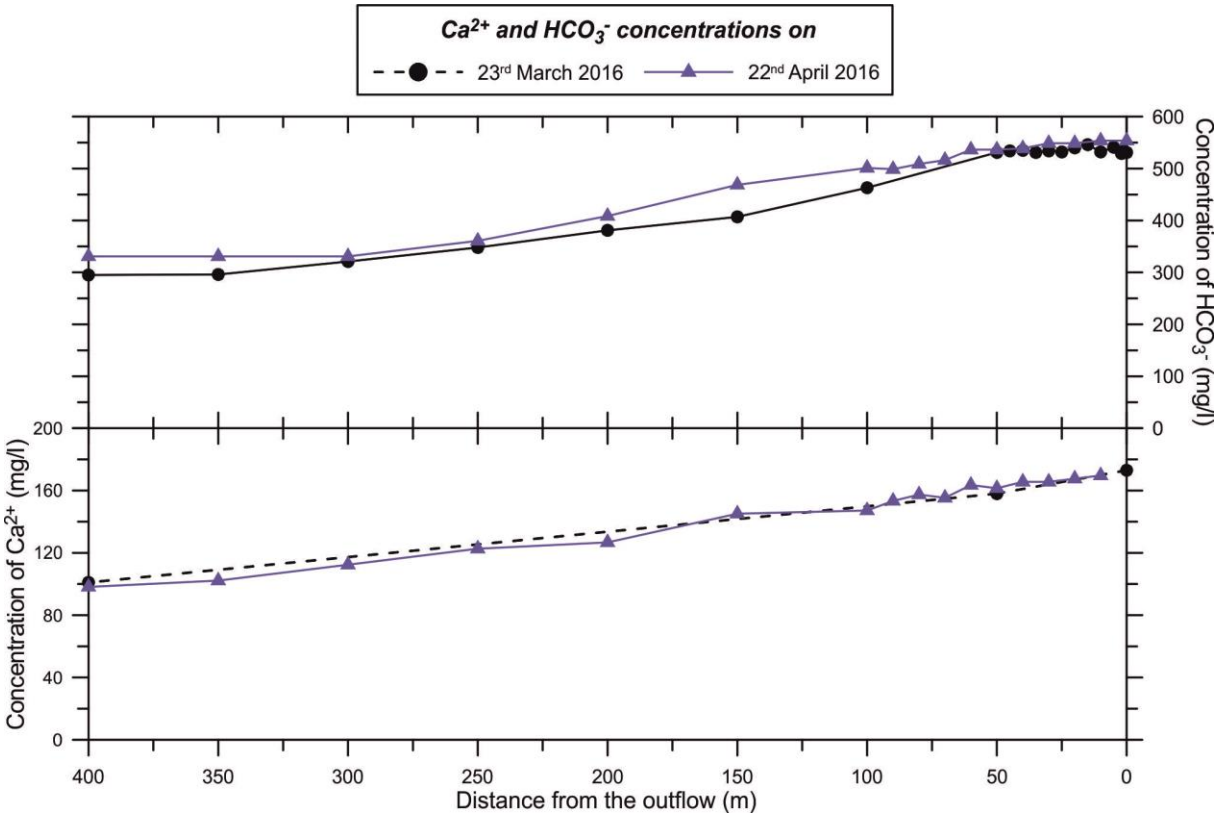

317

318 **Fig. 6** Variations in the concentrations of Ca^{2+} and HCO_3^- along the flow path (error of
319 measurements for both ions: 2 %)

320 **Table 2** Concentrations of the major ions at 0, 50 and 400m in April (error of measurements:
321 2 %, for SO_4^{2-}: 5 %)

Distance from the outflow (m)	SO_4^{2-} (mg/l)	Cl^- (mg/l)	Ca^{2+} (mg/l)	Mg^{2+} (mg/l)	Na^+ (mg/l)	K^+ (mg/l)
0	353	147	173	58	119	17

50	295	147	158	58	121	17
400	336	153	101	58	128	19

4.2 ^{226}Ra and ^{222}Rn activity

The concentration of ^{226}Ra in the water (mean value: 351 mBq/l) remained the same along the flow path within the error of analysis (Fig. 7).

The ^{222}Rn activity decreased from 167±9 Bq/l to 3±2 Bq/l (between the pit and the 400-metre point) with an increase at 20m in April. It dropped to the level of the background radiation (2–3 Bq/l) at 100 m (Fig. 7).

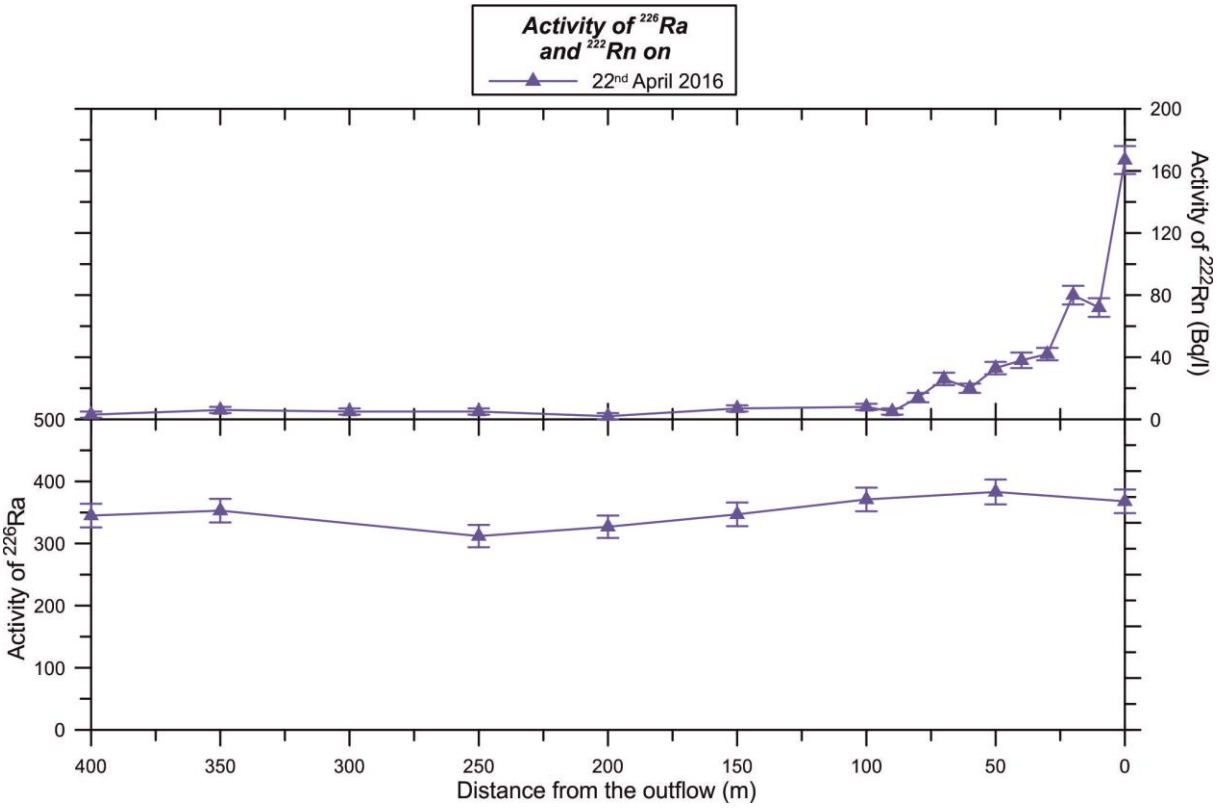

Fig. 7 Variations in the activity of ^{226}Ra and ^{222}Rn along the flow path

4.3 Trace elements

The concentration of trace elements in the original (unfiltered) samples and in the suspended solid (=unfiltered-filtered) are depicted in Fig. 8. Be, Bi, Cd, Cr, Hg, Mo, Pb, Sb, Sn, Te, Th,

Tl, U, V and Y were present at the lowest concentration in both the unfiltered samples and in the suspension, between 0 and 0.5 µg/l (Fig. 8a). Bi, Cr and Th were below the detection threshold in the filtered samples. The concentrations of Al, As, Cu, P, Sc, Se, Ti and Zn fell within the range of 1 to 12 µg/l (Fig. 8b), while Ba, B, Br, Cs, Fe, I, Li, Mn and Rb were between 10 and 620 µg/l (Fig. 8c). The concentration of S and Si were the highest (4000–55000 µg/l) in both the unfiltered samples and in the suspension (Fig. 8d).

In the case of many elements (Be, Bi, Cd, Cr, Pb, Th, Tl, V, Y, Al, Cu, Se, Ti, Zn, Fe, Mn) the concentration in the suspension is close to the total concentration. Other elements like Mo, U, As, P, B, Li, S are represented in relatively less abundance in the suspended solid (Fig. 8).

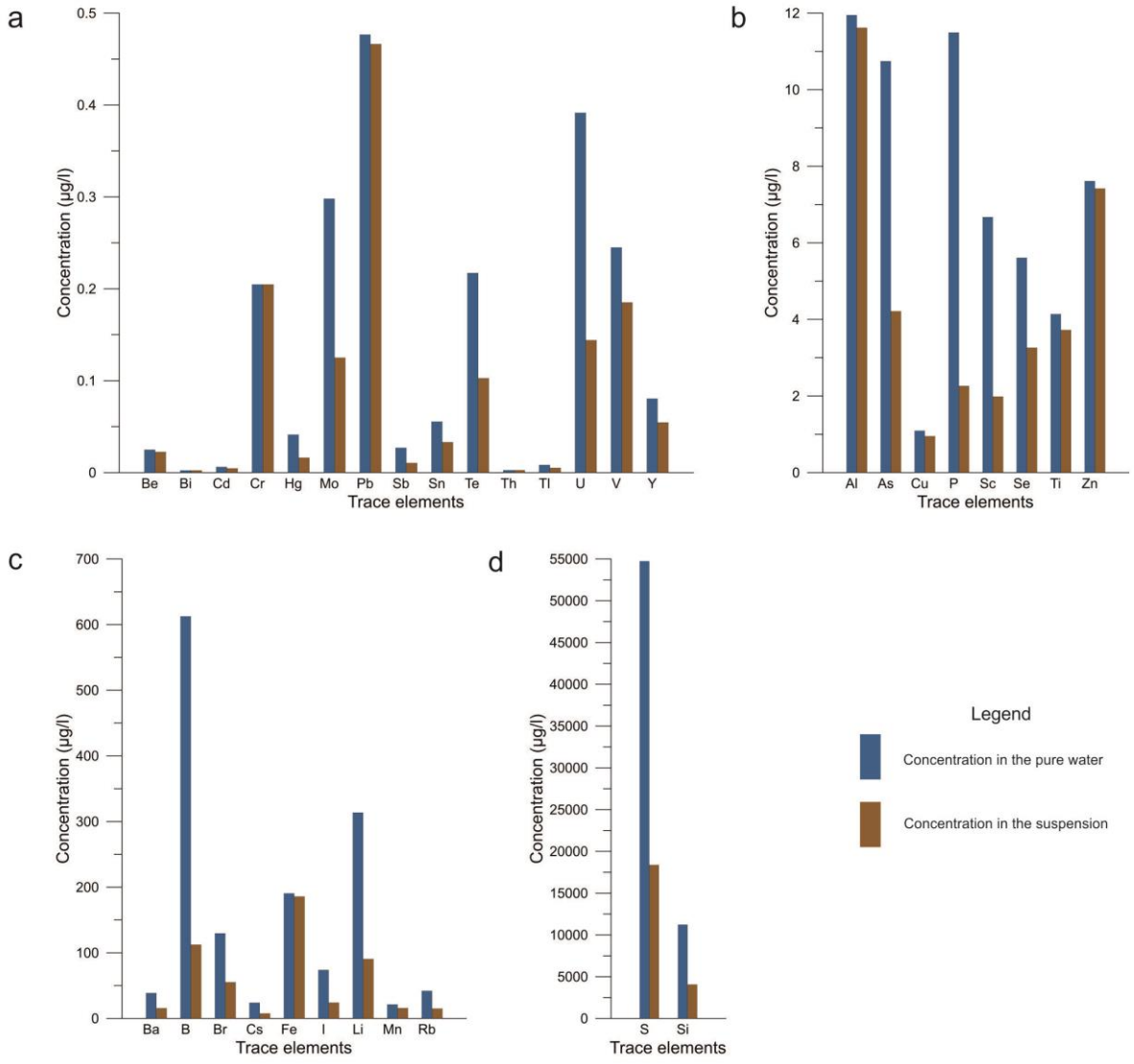

Fig. 8 Trace element concentrations in unfiltered water and in the suspended solid of the pit in the range of (**a**) 0–0.5, (**b**) 1–12, (**c**) 10–620, (**d**) 4000–55000 µg/l

4.4 Simulated $SI_{calcite}$ and p_{CO2} and reactive transport modelling

The saturation index with respect to calcite was modelled using the measured concentrations and parameters. The indices were positive along the whole flow path. The indices increased over the first 80m (0.4–1.55), then the values were almost the same between 80 and 150m (around 1.55), and decreased from 1.55 to 1.35 in the next 50m (150–200m), then remained around 1.35 (Fig. 9).

The partial pressure of CO_2 (p_{CO2}) changed in the opposite direction to $SI_{calcite}$. It steeply decreased in the first 100m, then, increased slightly in the next 100m (100–200m), and slightly decreased between 200 and 400m (Fig. 9).

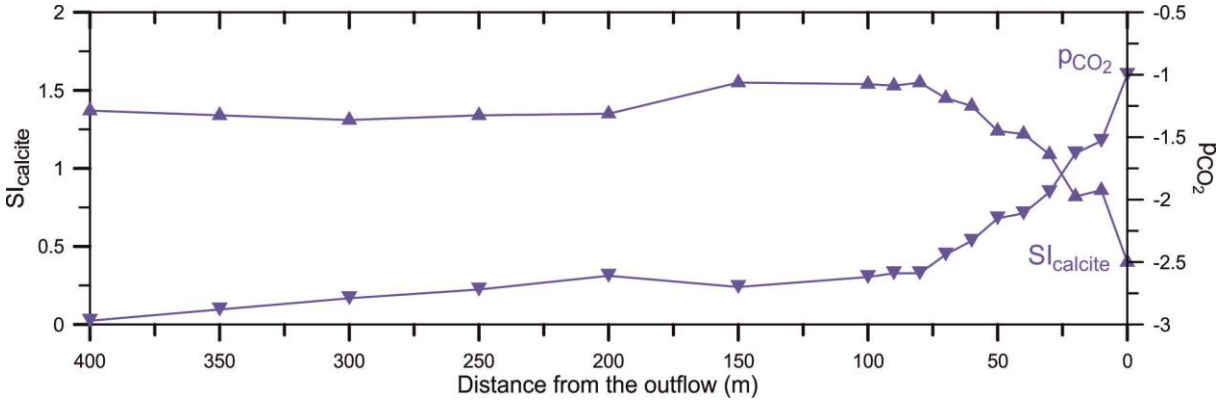

Fig. 9 Modelled variations in $SI_{calcite}$ and p_{CO2} along the flow path

The reactive transport model was fitted to the measured data using a model optimisation software, PEST (Watermark Numerical Computing, 2016), by adjusting the gas exchange rate constants for CO_2, O_2 and ^{222}Rn (k_{CO2}, k_{O2}, k_{Rn}) and the surface area over volume parameter (A/V) in the rate expression of calcite. While k_{O2} and k_{Rn} could be fitted to the data independently, it was found during trial runs that the value of k_{CO2} correlated to the value of

A/V in the expression of the rate for calcite precipitation. It was found that because of this dependence, a better fit of the measured pH values, which are very sensitive to the value of k_{CO2}, could only be obtained at the expense of a worse fit of the Ca^{2+} and HCO_3^- concentrations.

Flow and solute transport were modelled using the following form of the advection-dispersion equation, Eq. (2):

$$\frac{\partial m}{\partial t} = -v\frac{\partial m}{dx} + D_L\frac{\partial^2 m}{dx^2} + r \quad (2)$$

Where m is the aqueous concentration (M), t is time (s), v is the water flow velocity (m/s), x is the distance from the outflowing (m), and D_L is the hydrodynamic dispersion coefficient, which is defined as $D_L = \alpha_L v + D_e$ (m^2/s), where α_L is the dispersivity (m) and D_e is the diffusion coefficient (m^2/s).

The value of v was derived from the discharge rates measured in the course of the experiment. For D_e a value of 5×10^{-9} m/s^2 was assumed, and α_L was set to 0.05 m. No further optimization of these parameters was attempted, as a good fit between the modelled and measured ^{222}Rn could be obtained with these chosen values (Fig. 10). Since ^{222}Rn is chemically inert, this was considered to be confirmation of the model's ability to simulate the flow and mixing processes within the canal.

4.5 Observation of evolved precipitates

Due to six weeks of thermal water flowing, reddish-brown, amorphous precipitate formed close to the outflow, and up to distance of 15 m from it (Fig. 10a). Low magnification SEM images showed extended bacterial colonization, with some minerals in the first 15m-long section (Fig. 10b). The high-resolution SEM images reflected the networked structures and morphological variability of the biofilm-forming bacterial cells. Different sized and shaped

385 filamentous bacteria in interwoven form (red arrow), numerous straight (yellow arrow) and
386 curved rod-shaped (blue arrow), aggregate-forming cells of varied sizes (green arrow) were
387 visible in the photos. The rod-shaped cells form long chains (purple arrow) (Fig. 10c).

388 Downstream, a beige, crystalline precipitate evolved along to the end of the studied section
389 (Fig. 10d). Calcite crystals (also revealed by XRD) dominate this precipitate with serrated
390 mineral surfaces. In the low magnification SEM images, patches of bacterial colonization can
391 be seen (Fig. 10e). The morphology of bacteria of these colonizations is the same as in the
392 biofilms of the first 15 m (Fig. 10f).

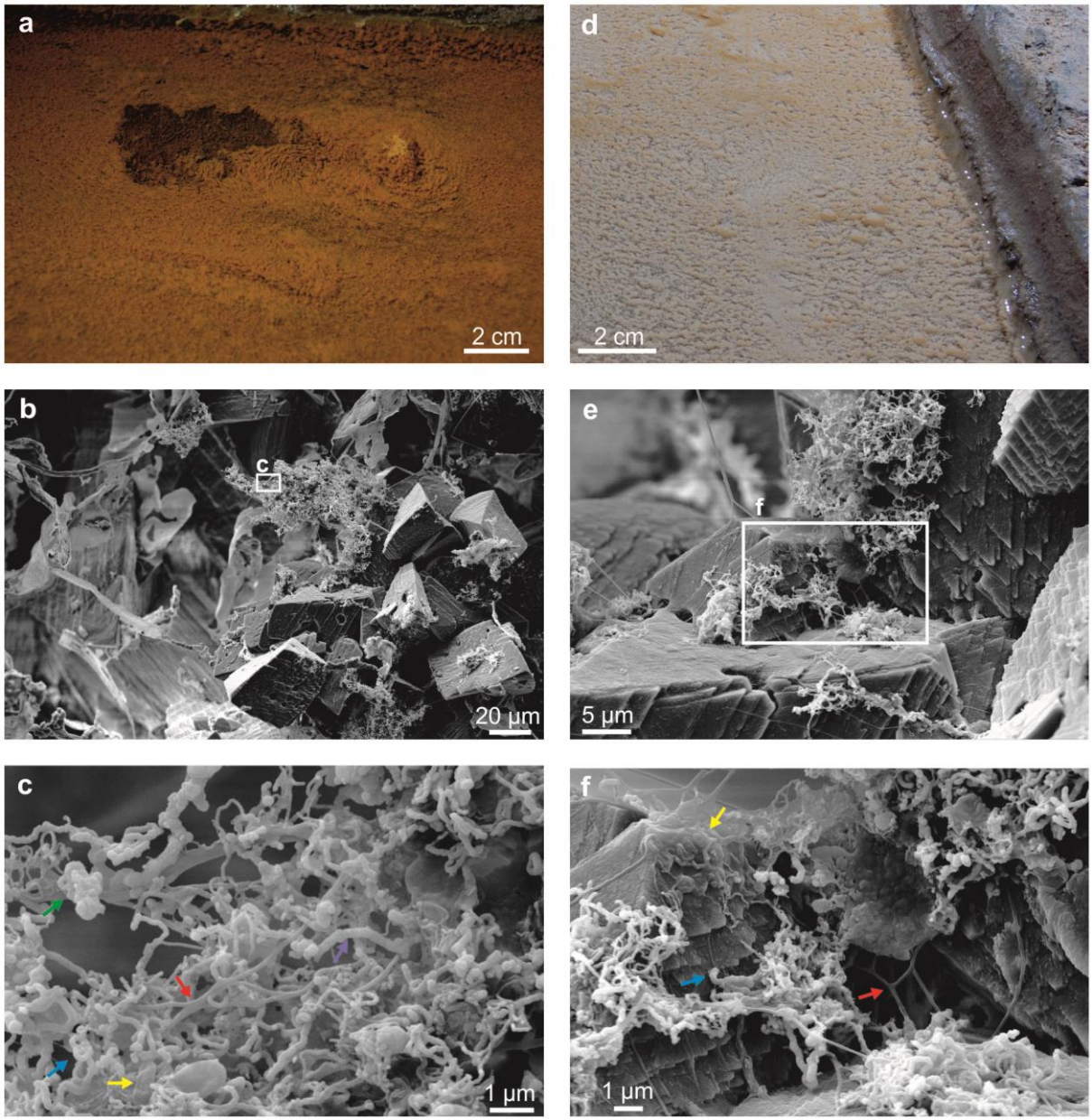

393

394 **Fig. 10** The reddish-brown, amorphous precipitate at 8 m **(a)** on site, **(b) (c)** in SEM images;

395 crystalline precipitate at 40 m **(d)** on site, **(e) (f)** in SEM images

396 **5. Interpretation and discussion**

397 Thermal springs are discharge features of regional groundwater flow systems and are

398 characterized by a near constant volume discharge and relatively invariant physicochemical

399 parameters at the outflow as long as the hydrogeological environment is stable (for hundreds

400 or thousands of years) (Goldscheider et al., 2010; Mádl-Szőnyi and Tóth, 2015). The natural

401 thermal water discharge can be simulated by invariable pumping from a well. Though the
402 initial discharge is stable, volume discharge could change along the flow path due to the
403 roughness and route of the bed, even in regular channels, like that in the experiment.

404 **5.1 Physicochemical parameter changes along the flow path**

405 The air temperature of the tunnel is affected by ventilation, but this fact does not necessarily
406 influence the temperature of the water inside the tunnel if the temperature of the water and the
407 air are similar, as was the case in the present study. This supposition was then confirmed by
408 the absence of significant correlation (-0.27) (Table 3).

409 **Table 3** Correlation matrix (Pearson correlation) for the measured parameters in March
410 (black) and April (blue) (n/a invalid values because the measured parameters are used for the
411 calculation of the modelled ones; * correlation is significant at the 0.05 level (two-tailed); (20)
412 number of data pairs)

	Water temperature	Air temperature	pH	Dissolved oxygen content	Specific electric conductivity	Concentration of Ca^{2+}	Concentration of HCO_3^-	^{226}Ra activity	^{222}Rn activity	$SI_{calcite}$	p_{CO_2}
Water temperature	1										
Air temperature		1									
	-0.27 (17)										
pH	-0.91* (20)		1								
	-0.87* (17)	0.63* (17)									
Dissolved oxygen content	-0.90* (20)		0.98* (20)	1							
	-0.87* (17)	0.68* (17)	0.95* (17)								
Specific electric conductivity	0.87* (20)		-0.89* (20)	-0.84* (20)	1						
	0.76* (17)	-0.23 (17)	-0.79* (17)	-0.76* (17)							
Concentration of Ca^{2+}						1					
	0.60* (16)	0.01 (16)	-0.72* (16)	-0.73* (16)	0.98* (16)						
Concentration of HCO_3^-	0.64* (20)		-0.67*	-0.58* (20)	0.92* (20)		1				

			(20)								
	0.50* (17)	-0.19 (17)	-0.66* (17)	-0.56* (17)	0.90* (17)	0.99* (16)					
^{226}Ra activity								1			
	0.19 (8)	-0.35 (8)	-0.41 (8)	-0.40 (8)	0.46 (8)	0.52 (7)	0.70 (8)				
^{222}Rn activity									1		
	0.86* (17)	-0.69* (17)	-0.96* (17)	-0.99* (17)	0.75* (17)	0.68* (16)	0.56* (17)	0.41 (8)			
$SI_{calcite}$	n/a		n/a			n/a	n/a			1	
		0.72* (17)		0.92* (17)	-0.57* (17)			-0.28 (8)	-0.94* (17)		
p_{CO2}	n/a		n/a								1
		-0.58* (17)		-0.94* (17)	0.85* (17)	0.80* (16)	0.74* (17)	0.46 (8)	0.94* (17)	-0.90* (17)	

n/a invalid values because the measured parameters are used for the calculation of the modelled ones
* correlation is significant at the 0.05 level (2-tailed)
() number of data pairs

The abrupt pressure drop at the outflow results in rapid, intensive CO_2 degassing and a concomitant sharp rise in pH values close to the outflow, with less intensive degassing as the volume of CO_2 in the water decreases.

The strong significant negative correlation (-0.94) (Table 3) demonstrates the converse nature of the change in dissolved oxygen content from p_{CO2}, as O_2 originating in the air of the tunnel dissolves into the water. After reaching saturation point, the dissolved oxygen content remains stable (Fig. 5).

Given the increase in the pH of the water, supersaturation and the precipitation of $CaCO_3$ are to be expected, and this assumption gains support from the increase of $SI_{calcite}$ (Fig. 9), the decrease in specific electric conductivity (Fig. 5) and the decrease in the concentration of the

two major ions, Ca^{2+} and HCO_3^- (Fig. 6). The significant correlation coefficients of 0.98 and 0.90–0.92 obtained between the specific electric conductivity and the concentrations of Ca^{2+} and HCO_3^-, respectively, confirm that the decrease in these two ions causes the drop in specific electric conductivity. The concentration of Ca^{2+} and HCO_3^- displayed a continual decrease along the flow path.

From the relatively spaced-out measurements, it seems that the concentration of other major ions (Mg^{2+}, Na^+, K^+, Cl^-) remains relatively constant along the flow path (Table 1); this is related to the fact that they do not take part in precipitation processes. Though Mg-calcite has been determined as the main mineral phase of the carbonates in the spring caves of the BTK (Erőss, 2010), along the flow path a decrease in Mg^{2+} in the water was not detectable.

5.2 Radionuclides and trace elements in the water

The concentration of ^{226}Ra remains stable (Fig. 8a) in the canal, displaying no significant correlation with any of the parameters (Table 3). ^{222}Rn is the decay product of ^{226}Ra, and it degasses rapidly from water, since there is no additional supply along the flow path. The ^{222}Rn activity displays a strong significant correlation with p_{CO2} (0.94) and a strong significant negative correlation with pH (-0.96) and dissolved oxygen content (-0.99) (Table 3). The strong correlation with p_{CO2} demonstrates that ^{222}Rn degasses in a way similar to CO_2, as it is also a dissolved gas: its concentration dropped to the level of the background radiation within the first 100 m (Fig. 7). The high surface-to-volume-ratio of the water flowing in the canal also promotes the processes of degassing and ingassing.

Erőss (2010) found that Ca, together with smaller amounts of Si, Mg, Fe and Al, was a main element in the build-up of biofilms in the spring caves in Gellért Hill. In a comprehensive study of the water in spring caves of BTK, S and Sr were found to have the highest concentrations (10–34.5 and 0.705–3.1 μg/l, respectively) among the trace elements (Dobosy

et al., 2016). In agreement with these findings, in this study S and Si were the main trace elements both in the water and in the suspended solid (Fig. 8d). Al, Be, Cd, Cr, Cu, Fe, Mn, Pb, Ti and Zn prefer the suspension form in the pit (Fig. 8). These elements were found to be in high concentrations in precipitates in the BTK (Dobosy et al., 2016; Erőss, 2010). This observation can be explained by the hydrolysis of the metal ions and their subsequent precipitation as hydroxides. Except for Li, these elements are abundant in the dissolved phase form of soluble oxoions (e.g. UO_2^{2+}, PO_4^{3-}, etc.). Thus, the distribution of the trace elements between dissolved and suspended matter can be accounted for.

5.3 Comparison of the measured and modelled variations of the parameters

The simulated values for dissolved oxygen and ^{222}Rn activity derived from the reactive transport model are in good agreement with the measured values for both the March and April experiments (Fig. 11). The pH values and HCO_3^- concentrations, on the other hand, do not match those of the model to such a degree. The March and April data show little change in the measured HCO_3^- concentration over the first 50m of the canal, whereas in the model, HCO_3^- concentrations decrease almost immediately. For Ca^{2+}, the opposite appears to be the case: the measured concentrations show an almost linear decrease starting immediately, albeit there is a wide scatter of the data points in April, while the modelled Ca^{2+} decrease along the canal seems to be slow initially, becoming progressively faster further downstream. The model consistently underestimates pH. Obtaining a better fit of the pH by using a faster CO_2 degassing rate only worsened the fit for Ca^{2+}. Finally, from the measurements it appears that the decrease in HCO_3^- stabilises after 300–350 m, and this is more clearly apparent in the April data. While the model similarly predicts a lower rate of decrease with downstream distance, the change in the simulated concentration-versus-distance curve is much more gradual, and not as pronounced as for the measured concentrations (Fig. 11).

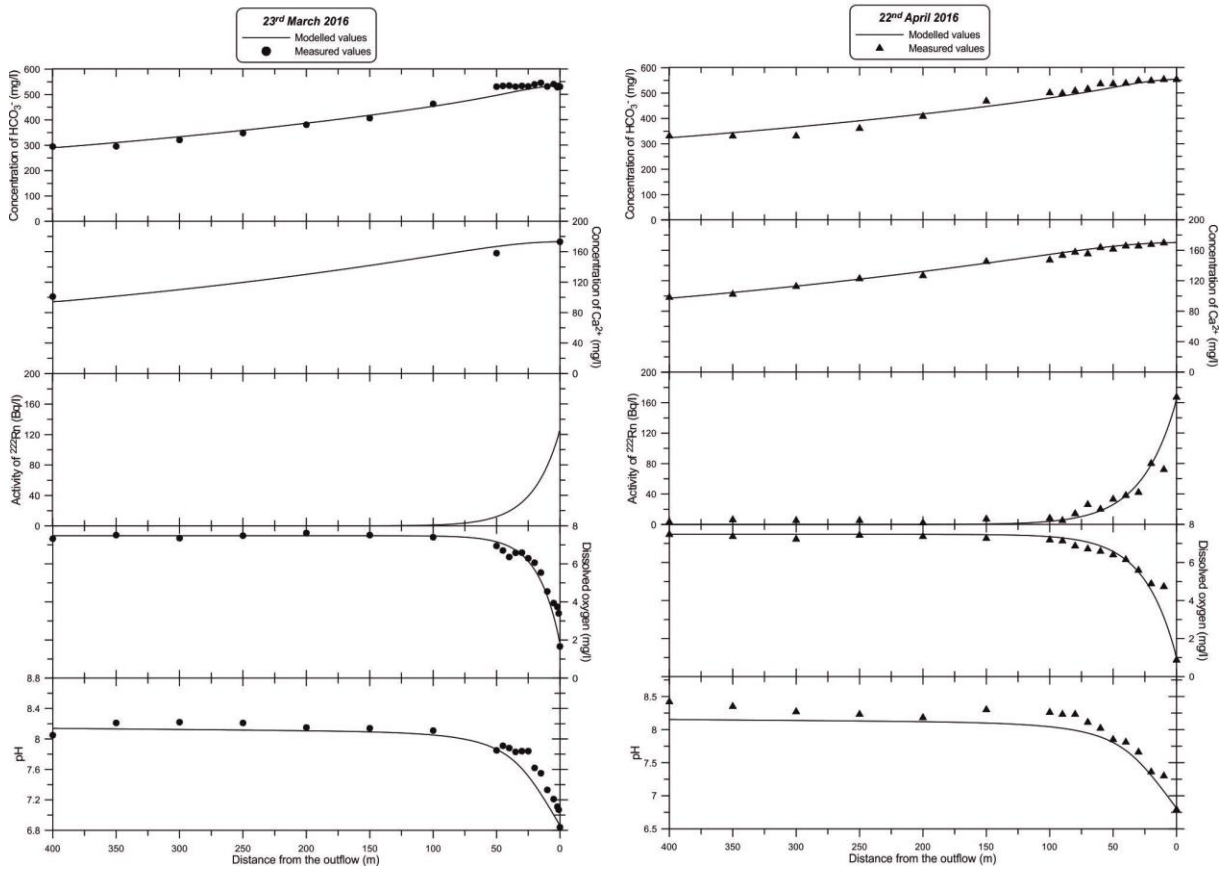

472

473 **Fig. 11** The measured and modelled variations of pH, dissolved oxygen, ^{222}Rn activity, and

474 Ca^{2+} and HCO_3^- concentrations along the flow path

475 **5.4 Indirect and direct indications and evidences for biological and carbonate**

476 **precipitation**

477 According to Eq. (3) one mole of Ca^{2+} reacts with two equivalent alkalinity (indicated as

478 HCO_3^-), so the stoichiometric ratio of Ca:alkalinity is 1:2 (Eq. (3)). The blue line in Fig. 12.

479 shows this ratio.

480 $$2HCO_3^- + Ca^{2+} \rightarrow CaCO_3 + 2H^+ \quad (3)$$

481 The variations in the concentrations of the two major ions show that the ratio changes in the

482 way described by Eq. (3) until 150 m from the outflow. After 150 m, less HCO_3^- or more Ca^{2+}

483 leaves the water (Fig. 12.), what is consumed in calcite precipitation.

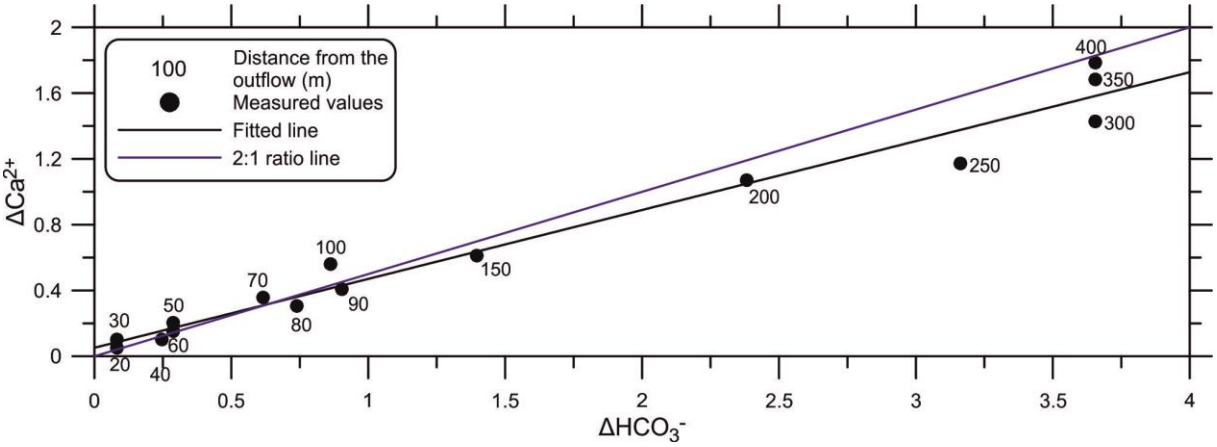

Fig. 12 Changes in Ca^{2+} and HCO_3^- along the flow path

The variations in the concentrations of major ions and specific electric conductivity, the measured Ca:alkalinity ratio and the simulations refer to continuous calcium carbonate precipitation along the flow path. The stoichiometric ratio of Ca:alkalinity of the measured major ions and the reactive transport model shows adverse HCO_3^- concentration compared to the equation and simulated values. It suggests that after 150 m from the outflow, beside $CaCO_3$ precipitation, the simulated gas exchange, namely CO_2 degassing decreases the dissolved HCO_3^- concentration. However, another process is supposed to further reduce it. A possible explanation is the roughness/shallowing of the canal bed (Hammer et al., 2008).

The afore-mentioned changes of physicochemical parameters are the results of the one-day-long experiments, when thermal water was pumped into the canal, where no precipitates were to be found. Though there are indications of $CaCO_3$ precipitation, carbonates could not be observed in the canal after one day. Bacteria arriving with the thermal water also could not form any biofilm during the limited duration of the experiment. Consequently, the effects of the precipitates could not be examined in this part of the study.

The increase in pH and the decrease in the concentration of Ca^{2+} and HCO_3^- can be observed along the flow path in travertine-depositing streams and springs (Amundson and Kelly, 1988;

Dandurand et al., 1982; Herman and Lorah, 1986, 1987; Hoffer-French & Herman, 1989, 1990; Lorah and Herman 1988, 1990; Nordstrom et al., 2005 etc.). In many cases, physical evidence (e.g. travertines) for calcite precipitation are to be seen in springs, where the streambed is steep and especially around waterfalls (Chen et al., 2004; Zhang et al., 2001),. In such places, calcite supersaturation by at least a factor of five is required for calcite precipitation (Hoffer-French and Herman 1989, 1990; Jacobson & Usdowski, 1975; Lorah and Herman 1988, 1990).

According to the observations of the formed precipitates during the 6-weeks-long experiment, there is continuous precipitation along the flow path, dominated by bacteria close to the outflow and by calcite further downstream. The change from the organic to the inorganic precipitate is to be found in the abruptly changing section of physicochemical parameters. The appearance of the reddish-brown biofilm is consistent with the field observations, that biofilms are forming at the mixing of reduced thermal water and oxidative air (Borsodi et al., 2012; Erőss et al., 2012; Mádl-Szőnyi and Erőss, 2013; Mádl-Szőnyi et al., 2017a). The reddish-brown colour is the usual colour of biofilms in the BTK, caused by Fe(III), refers to the presence of iron(FeII)-oxidizing bacteria (Anda et al., 2014; Borsodi et al., 2012).

In the experimental canal, from 15 m downstream, calcite precipitates, also the parameters became stable. At the beginning of this section $SI_{calcite}$ is 0.82–0.86, which means that this rate of supersaturation is required for calcite precipitation under the circumstances of the experiment. Inorganic processes seem to control the precipitation and they suppress organic ones after 15 m from the outflow. It was revealed by SEM images, where patches of biofilms can be seen on the surfaces of calcite crystals.

It seems that in the scale and time period of the measurements and observations, there is no evidence for the effect of bacteria on calcite precipitation and changes of aquatic chemistry.

The study of the interrelationships between water chemistry and the precipitates needs longer time scale, which was not part of this study.

6. Conclusions and summary

Springs display changes in their physicochemical parameters from their discharge along their flow path. The main driving force of these changes is the pressure drop, resulted in CO_2 degassing. The variations have a direct effect on the formation of organic and inorganic precipitates. The complexity of natural spring systems and the limitations of laboratory experiments make it difficult to understand all the governing factors. In situ experiments, integrated with reactive transport modelling, provide a useful tool to monitor the physicochemical parameters and to better understand the background processes.

The in situ experimental study, carried out in the canal of the Gellért tunnel, BTK, was conducted to simulate thermal spring discharge into a warm-air cave.It was found that the main driving forces of the physicochemical parameter changes along the flow path areCO_2 degassing and in this context, calcite precipitation. The latter had no physical evidence after the one-day-long experiment, only indirect indications, namely the gradual decrease in specific electric conductivity, Ca^{2+} and HCO_3^- concentrations and increase in pH and $SI_{calcite}$.

Due to the high gradient between the air and the water, the changes are fast and occur in the first 100 m from the outflow. The temperature difference between water and air temperatures is a less influential factor in the changes in the parameters and $SI_{calcite}$.The dissolving of oxygen from the air into the water, and the degassing of ^{222}Rn are controlled by pure chemical reactions, as was also confirmed by reactive transport model. Beside the modelled CO_2 degassing and calcite precipitation, another process influences pH and the concentration of HCO_3^-, which is probably the roughness of the stream bed. In the scale and time period of the in situ experiments, the effect of bacteria and calcite precipitation could not be detected.

In the absence of organic and inorganic precipitates, most of the trace elements which are usually adsorbed by biofilm occurring in the natural spring caves of the BTK, were present in the form of suspended solids in the water, a fact which seems to be related to early precipitation processes. The activity of ^{226}Ra in the water remained stable along the flow path in the lack of adsorbing precipitates.

The presence of bacteria in the form of biofilm close to the outflow was observed after six weeks of the flow of the same thermal water as used in the experiment. The appropriate circumstances for bacteria forming biofilm is where thermal water discharges and interacts with the oxidative air. Reddish brown colour reflects the presence of iron(FeII)-oxidizing bacteria.

In the circumstances of the experiment, supersaturation levels of 0.82–0.86 with respect to calcite proved to be sufficient for precipitation. The key to the change from biological to chemical precipitates is to be found in the abruptly changing section of physicochemical parameters. The precipitation of calcite continued after the parameters became stable. Further downstream inorganic processes suppress microbiological life, and bacterial colonization could be observed only patchily on the surface of calcite crystals.

This study was able to demonstrate that a method integrating experimental study, numerical modelling is a suitable approach in the quest to understand precipitation processes around thermal springs better.

References

Alföldi L, Bélteky L, Böcker T, Horváth J, Korim K, Rémi R (eds) (1968) Budapest hévizei (Thermal waters of Budapest) [in Hungarian]. Hungarian Institute for Water Resources Research Budapest, Budapest

573 Amundson R, Kelly E (1987) The chemistry and mineralogy of a CO_2-rich travertine
574 depositing spring in the California Coast Range. Geochim Cosmochim Acta 51:2883–2890.
575 doi: 10.1016/0016-7037(87)90364-4

576 Anda D, Büki G, Krett G, Makk J, Márialigeti K, Erőss A, Mádl-Szőnyi J, Borsodi AK
577 (2014) Diversity and Morphological structure of bacterial communities inhabiting the Diana-
578 Hygieia thermal spring (Budapest, Hungary). Acta Microbiol Immunol Hun 61(3):329–346.
579 doi: 10.1556/AMicr.61.2014.3.7

580 Anda D, Makk J, Krett G, Jurecska L, Márialigeti K, Mádl-Szőnyi J, Borsodi AK (2015)
581 Thermophilic prokaryotic communities inhabiting the biofilm and well water of a thermal
582 karst system located in Budapest (Hungary). Extremophiles 19(4):787–797. doi:
583 10.1007/s00792-015-0754-1

584 Borsodi AK, Knáb M, Krett G, Makk J, Márialigeti K, Erőss A, Mádl-Szőnyi J (2012)
585 Biofilm Bacterial Communities Inhabiting the Cave Walls of the Buda Thermal Karst System,
586 Hungary. Geomicrobiol J 29(7):611–627. doi: 10.1080/01490451.2011.602801

587 Chen J, Zhang DD, Wang S, Xiao T, Huang R (2004) Factors controlling tufa deposition in
588 natural waters at waterfall sites. Sediment Geol 166:353–366. doi:
589 10.1016/j.sedgeo.2004.02.003

590 Dandurand JL, Gout R, Hoefs J, Menschel G, Schott J, Usdowski E (1982) Kinetically
591 controlled variations of major components and carbon and oxygen isotopes in a calcite-
592 precipitating spring. Chem Geol 36:299–315. doi: 10.1016/0009-2541(82)90053-5

593 Das S, Mohanti M (2015) The geochemistry of tufa-depositing stream waters of Bhaliadal,
594 Mayurbhanj District (Odisha), India. Vistas Geol Res Spec Publ Geol 13:141–151.

595 Dobosy P, Sávoly Z, Óvári M, Mádl-Szőnyi J, Záray Gy (2016) Microchemical
596 characterization of biogeochemical samples collected from the Buda Thermal Karst Sytem,
597 Hungary. Microchem J 124:116–120. doi: 10.1016/j.microc.2015.08.004

598 Dreybrodt W, Buhmann D, Michaelis J, Usdowski E (1992) Geochemically controlled calcite
599 precipitation by CO_2 outgassing: Field measurements of precipitation rates in comparison to
600 theoretical predictions. Chem Geol 97:285–294. doi: 10.1016/0009-2541(92)90082-G

601 Eaton AD, Clesceri LS, Rice EW, Greenberg AE, Franson MAH (eds) (2005) Standard
602 methods for the examination of water and wastewater, 21st edn. American Public Health
603 Association, Washington DC

604 Ehrlich HL (2001) Geomicrobiology, 4th edn. Marcel Dekker, New York

605 Engel AS, Porter ML, Kinkle BK, Kane TC (2001) Ecological Assessment and Geological
606 Significance of Microbial Communities from Cesspool Cave, Virginia. Geomicrobiol J
607 18(3):259–274. doi: 10.1080/01490450152467787

608 Erhardt I, Ötvös V, Erőss A, Czauner B, Simon Sz, Mádl-Szőnyi J (2017) Hydraulic
609 evaluation of the hypogenic karst area in Budapest (Hungary). Hydrogeol J 25(6): 1871–1891.
610 doi: 10.1007/s10040-017-1591-3

611 Erőss A (2010) Characterization of fluids and evaluation of their effects on karst development
612 at the Rózsadomb and Gellért Hill, Buda Thermal Karst, Hungary. Dissertation, Eötvös
613 Loránd University

614 Erőss A, Mádl-Szőnyi J, Surbeck H, Horváth Á, Goldscheider N, Csoma ÉA (2012)
615 Radionuclides as natural tracers for the characterization of fluids in regional discharge areas,
616 Buda Thermal Karst, Hungary. J Hydrol 426–427:124–137. doi:
617 10.1016/j.jhydrol.2012.01.031

618 Fujisawa A, Tazaki K (2003) The radioactive microbial mats – In case of Misasa hot springs
619 in Tottori Prefecture. In: Kamata N (ed): Proceedings: International Symposium of the
620 Kanazawa University 21st-Century COE Program Vol1. Kanazawa University, Kanazawa,
621 Japan, pp 328–331

622 Gainon F, Goldscheider N, Surbeck H (2007) Conceptual model for the origin of high radon
623 levels in spring waters – the example of the St. Placidus spring, Grisons, Swiss Alps. Swiss J
624 Geosci 100:251–262. doi: 10.1007/s00015-007-1220-6

625 Genereux DP, Hemond HF (1992) Determination of gas exchange rate constants for a small
626 stream on Walker Branch Watershed, Tennessee. Water Resour Res 28(9):2365-2374. doi:
627 10.1029/92WR01083

628 Goldscheider N, Mádl-Szőnyi J, Erőss A, Schill E (2010) Review: thermal water resources in
629 carbonate rock aquifers. Hydrogeol J 18(6):1303–1318. doi: 10.1007/s10040-010-0611-3

630 Haas J (2001) Geology of Hungary. Eötvös University Press, Budapest

631 Hammer Ø, Dysthe DK, Lelu B, Lund H, Meakin P, Jamtveit B (2008) Calcite precipitation
632 instability under laminar, open-channel flow. Geochim Cosmochim Acta 72:5009–5021., doi:
633 10.1016/j.gca.2008.07.028

634 Herman JS, Lorah MM (1986) Groundwater geochemistry in Warm River Cave, Virginia.
635 NSS Bull 48:54–61.

636 Herman JS, Lorah MM (1987) CO_2 outgassing and calcite precipitation in Falling Spring
637 Creek, Virginia, U.S.A. Chem Geol 62:251–262., doi: 10.1016/0009-2541(87)90090-8

638 Hoffer-French KJ, Herman JS (1989) Evaluation of hydrological and biological influences on
639 CO2 fluxes from a karst stream. J Hydrol 108:189–212. doi: 10.1016/0022-1694(89)90283-7

640 Hoffer-French KJ, Herman JS (1990) A CO_2 outgassing model for Falling Spring Run,
641 Augusta County, Virginia. In: Herman JS, Hubbard JrA (eds) Travertine-marl: stream
642 deposits in Virginia. Virginia Div Mineral Res Publ 101, pp 17–32

643 Jacobson RL, Usdowski E (1975) Geochemical controls on a calcite precipitating spring.
644 Contrib Mineral Petrol 51:65–74. doi: 10.1007/BF00403513

645 Keppel MN, Post VEA, Love AJ, Clarke JDA, Werner AD (2012) Influences on the
646 carbonate hydrochemistry of mound spring environments, Lake Eyre South region, South
647 Australia. Chem Geol 296–297:50–65. doi: 10.1016/j.chemgeo.2011.12.017

648 Kovács J, Erőss A (2017) Statistically optimal grouping using combined cluster and
649 discriminant analysis (CCDA) on a geochemical database of thermal karst waters in Budapest.
650 Appl Geochem 84:76–86, doi: 10.1016/j.apgeochem.2017.05.009

651 Leél-Őssy Sz (1995) A Rózsadomb és környékének különleges barlangjai (Special caves of
652 Rózsadomb on Buda and its environs) [in Hungarian]. Földt Közl 125 (3–4):363–432.

653 Leél-Őssy Sz, Surányi G (2003) Peculiar hydrothermal caves in Budapest, Hungary. Acta
654 Geol Hung 46:407–436., doi: 10.1556/AGeol.46.2003.4.5

655 Le Guern C, Baranger P, Crouzet C, Bodénan F, Conil P (2003) Arsenic trapping by iron
656 oxyhydroxides and carbonates at hydrothermal spring outlets. Appl Geochem 18:1313–1323.,
657 doi: 10.1016/S0883-2927(03)00053-2

658 Lorah MM, Herman JS (1988) The chemical evolution of a travertine-depositing stream:
659 Geochemical processes and mass-transfer reactions. Water Resour Res 24(9):1541–1552.,
660 doi: 10.1029/WR024i009p01541

661 Lorah MM, Herman JS (1990) Geochemical evolution and calcite precipitation rates in
662 Falling Spring Creek, Virginia. In: Herman JS, Hubbard JrA (eds) Travertine-marl: stream
663 deposits in Virginia. Virginia Div Mineral Res Publ 101, pp 5–17

664 Makk J, Tóth E, Anda D, Pál S, Schumann P, Kovács AL, Mádl-Szőnyi J, Márialigeti K,
665 Borsodi AK (2016) Deinococcus budaensis sp. nov., a mesophilic species isolated from
666 biofilm sample of a hydrothermal spring cave. Int J Syst Evol Microbiol 66(12):5345–5351.,
667 doi: 10.1099/ijsem.0.001519

668 Mádl-Szőnyi J, Czauner B, Iván V, Tóth Á, Simon Sz, Erőss A, Bodor P, Havril T, Boncz L,
669 Sőreg L (2017b) Confined carbonates – regional scale hydraulic interaction or isolation? Mar
670 Pet Geol. doi: 10.1016/j.marpetgeo.2017.06.006

671 Mádl-Szőnyi J, Erőss A (2013) Effects of regional groundwater flow on deep carbonate
672 systems focusing on discharge zones. Proceedings of the International Symposium on
673 Regional Groundwater Flow: Theory, Applications and Future development. 21-23 June
674 Xi'an, China. China Geological Survey, Commission of Regional Groundwater Flow, IAH,
675 71-75.

676 Mádl-Szőnyi J, Erőss A, Tóth Á (2017a) Fluid flow systems and hypogene karst of the
677 Transdanubian Range, Hungary – With special emphasis on Buda Thermal Karst. In:
678 Klimchouk A, Palmer A, De Waele J, Auler A, Audra P (eds) Hypogene Karst Regions and
679 Caves of the World, Springer. doi: 10.1007/978-3-319-53348-3

680 Mádl-Szőnyi J, Leél-Őssy Sz, Kádár M, Angelus B, Zsemle F, Erőss A, Kalinovits S, Segesdi
681 J, Müller I, Mindszenty A (2001) A Budai Termálkarszt-rendszer hidrodinamikájának
682 vizsgálata nyomjelzéssel. (The examination of the hydrodynamic situation of Buda Thermal
683 Karst with tracers) [in Hungarian]. (Report) Budapest, Hungary

Mádl-Szőnyi J, Tóth Á (2015) Basin-scale conceptual groundwater flow model for an unconfined and confined thick carbonate region. Hydrogeol J 23(7):1359–1380. doi: 10.1007/s10040-015-1274-x

Nagai K, Tazaki K, Tanaka Y (2001) Accumulation of arsenic in microbial mats, Masutomi springs, Yamanashi prefecture [in Japanese]. Geosci Rep Shimane Univ 20:179–188.

Nordstrom DK, Ball JW, McCleskey RB (2005) Ground water to surface water: Chemistry of thermal outflows in Yellowstone National Park. Geotherm Biol Geochem Yellowstone Natl Park 73–94.

Parkhurst DL, Appelo CAJ (2013) Description of input and examples for PHREEQC version 3—A computer program for speciation, batch-reaction, one-dimensional transport, and inverse geochemical calculations. U.S. Geological Survey Techniques and Methods, book 6, chap A43

Plummer LN, Wigley TML, Parkhurst DL (1978) The kinetics of calcite dissolution in CO_2–water systems at 5 degrees to 60 degrees C and 0.0 to 1.0 atm CO_2. Am J Sci 278(2):179-216., doi: 10.2475/ajs.278.2.179

Raymond PA, Zappa CJ, Butman D, Bott TL, Potter J, Mulholland P, Laursen AE, McDowell WH, Newbold D (2012) Scaling the gas transfer velocity and hydraulic geometry in streams and small rivers. Limnol Oceanogr: Fluid Environ 2(1):41-53., doi: 10.1215/21573689-1597669

Sarbu SM, Kane TC, Kinkle BK (1996) A Chemoautotrophically Based Cave Ecosystem. Science 272(5270):1953–1955., doi: 10.1126/science.272.5270.1953

Schafarzik F (1920) Szökevény hévforrások a Gellérthegy tövében (Springs discharging directly in River Danube) [in Hungarian]. Földt Közl 3:79–158.

Somogyi K (2009) A Duna hatása a Gellért-hegy előterében (The effect of River Danube at the foothill of Gellért Hill) [in Hungarian]. MSc Thesis, Eötvös Loránd University

Striczki I (2010) A Duna és a felszín alatti vizek kapcsolatának vizsgálata a budai Dunaparti Főgyűjtő csatorna monitoring rendszerébe tartozó kutak, források segítségével (The connection between River Danube and groundwater based on the observation wells and springs of the monitoring network of Main Sewer system of Danube bank on the Buda side) [in Hungarian]. MSc Thesis, Eötvös Loránd University

Surbeck H (2000) Alpha spectrometry sample preparation using selectively adsorbing thin films. Appl Radiat Isot 53:97–100., doi: 10.1016/S0969-8043(00)00119-6

Takács-Bolner K, Kraus S (1989) A melegvizes eredetű barlangok kutatásának eredményei (Results of research into caves with thermal water origins) [in Hungarian]. Karszt Barl I-II:61–66.

Tazaki K (2009) Observation of microbial mats in radioactive hot springs. Sci Rep Kanazawa Univ 53:25–37.

Tóth J (1963) A theoretical analysis of groundwater flow in small drainage basins. J Geophys Res 68:4795–4812., doi: 10.1029/JZ068i016p04795

Watermark Numerical Computing (2016) PEST - Model-Independent Parameter Estimation User Manual Part I: PEST, SENSAN and Global Optimisers.

Weidinger T, Nagy B, Mádlné Szőnyi J, Bodor P, Salavec P, Tordai Á (2016) Terepi mérések a Gellért-hegy belsejétől a Száraz Andokig (Field measurements from the inside of the Gellért Hill to the Dry Andes) [in Hungarian]. In: Pongrácz R, Mészáros R (eds) Kutatási és operatív feladatok meteorológusként (Research and operative challanges as a meteorologist). Egy Met Füz 27:162–172.

730 Zhang DD, Zhang Y, Zhu A, Cheng X (2001) Physical mechanisms of river waterfall tufa
731 (travertine) formation. J Sediment Res 71(1):205–216., doi: 10.1306/061600710205